ChemPubSoc Europe

DOI: 10.1002/chem.201403036

CHEMISTRY
A European Journal
Full Paper

Supramolecular Systems

One-Step Versus Multistep Equilibrium of Carbazole-Bridged Dinuclear Zinc(II) Complex Formation: Metal-Assisted π-Association and -Dissociation Processes

Norie Inukai, Tsuyoshi Kawai,* and Junpei Yuasa*[a]

Abstract: This work demonstrates a selection criteria that determines whether molecular assembly occurs through a one-step or stepwise manner in ligand-bridged dinuclear zinc(II) (Zn^{2+}) complex formation, which is associated with the π stacking of building blocks. The building blocks of carbazole ligands (**L**[1] and **L**[4]) that contain two imidazole moieties at the 3,6-positions form 4:2 complexes (i.e., $[L]_4$–$(Zn^{2+})_2$) at a molar ratio of 0.50 ($[Zn^{2+}]/[L]_0 = 0.50$), thereby providing π stacking between the carbazole ligands. At the molar ratio of 0.67 ($[Zn^{2+}]/[L]_0 = 0.67$), the 4:2 complexes change to 3:2 complexes (i.e., $[L]_3$–$(Zn^{2+})_2$) with no π-stacked carbazole unit. In contrast, when the imidazole groups in **L**[1] are replaced with benzoimidazole groups (**L**[3]), **L**[3] also yields the 4:2 complex $[(L^3)_4$–$(Zn^{2+})_2]$ at a molar ratio of 0.50. However, there is no structural transition from $(L^3)_4$–$(Zn^{2+})_2$ to other complex species above a molar ratio of 0.50. Similarly, when two imidazole groups are introduced into the carbazole ring at 2,7-positions (**L**[5]), **L**[5] also gives the 4:2 complex $[(L^5)_4$–$(Zn^{2+})_2]$ that shows no structural transition to other complex species at a higher molar ratio.

Introduction

Natural principles are based on the creation of vast libraries of structures from a limited number of building blocks in a simultaneous multistep assembly process, thereby achieving a high level of complexity.[1–3] The multistep assembly strategy is a powerful method for achieving structural diversity from simple covalent building blocks under thermodynamic control, in which multiple species can interconvert between two or more self-assembled structures through a relatively flat potential-energy surface (Scheme 1 a).[4–11] The delicate thermodynamic balance results in a multistep equilibrium system,[12–21] in which the concentration of each of the molecular constituents is determined by the concentrations and molar ratio of the primary building blocks. This leads to a single complex species at each respective molar ratio, which can undergo structural transition to the other assembled structures at different molar ratios (Scheme 1 a).[12,13] However, most molecular assembly strategies involve one-step equilibrium systems, which lead to a single thermodynamic product as a result of its much higher stability relative to the other members (Scheme 1 b).[22,23] In contrast, an almost flat energy landscape generates a complex mixture of products (Scheme 1 c). These classifications raise important questions: What are the selection criteria that determine whether molecular assembly occurs in one step or a stepwise manner? And how do building molecules lead to a single thermodynamic product at each respective molar ratio in the multistep mechanism under thermodynamic control? Once we answer these critical questions, it will open up the opportunity to rationally plan unique supramolecular systems for achieving high diversity in structures and organization from a limited number of building blocks.

In this work, these questions are addressed by investigating metal-assisted π-association and -dissociation processes in one step versus multistep formation of carbazole-bridged dinuclear complexes.[24–30] The carbazole ligand (**L**) forms a 4:2 complex $[(L)_4$–$(Zn^{2+})_2]$ at a molar ratio of zinc ions (Zn^{2+}) to the ligand of 0.50,[31–33] which provides the opportunity for π stacking between the carbazole ligands. In the multistep mechanism, the 4:2 complex undergoes a structural transition to a 3:2 complex $[(L)_3$–$(Zn^{2+})_2]$ at the higher molar ratio, thereby resulting in dissociation of π stacking between the carbazole ligands. Conversely, in the one-step mechanism, no clear structural transition into other complex species occurs, thus leading to $[(L)_4$–$(Zn^{2+})_2]$ as a single thermodynamic product. The π stacking between the carbazole ligands in the molecular assembly acts as a suitable noncovalent interaction motif to achieve a delicate thermodynamic balance between the multiple complex species.[34] Systematic comparison between the two mechanisms provides a valuable insight into how building molecules such as carbazole ligands are capable of providing a single thermodynamic product at each respective molar ratio in the stepwise mechanism.

[a] Dr. N. Inukai, Prof. Dr. T. Kawai, Dr. J. Yuasa
Graduate School of Materials Science
Nara Institute of Science and Technology
8916-5 Takayama, Ikoma, Nara 630-0192 (Japan)
Fax: (+81) 743-72-6179
E-mail: tkawai@ms.naist.jp
yuasaj@ms.naist.jp

Supporting information for this article is available on the WWW under http://dx.doi.org/10.1002/chem.201403036.

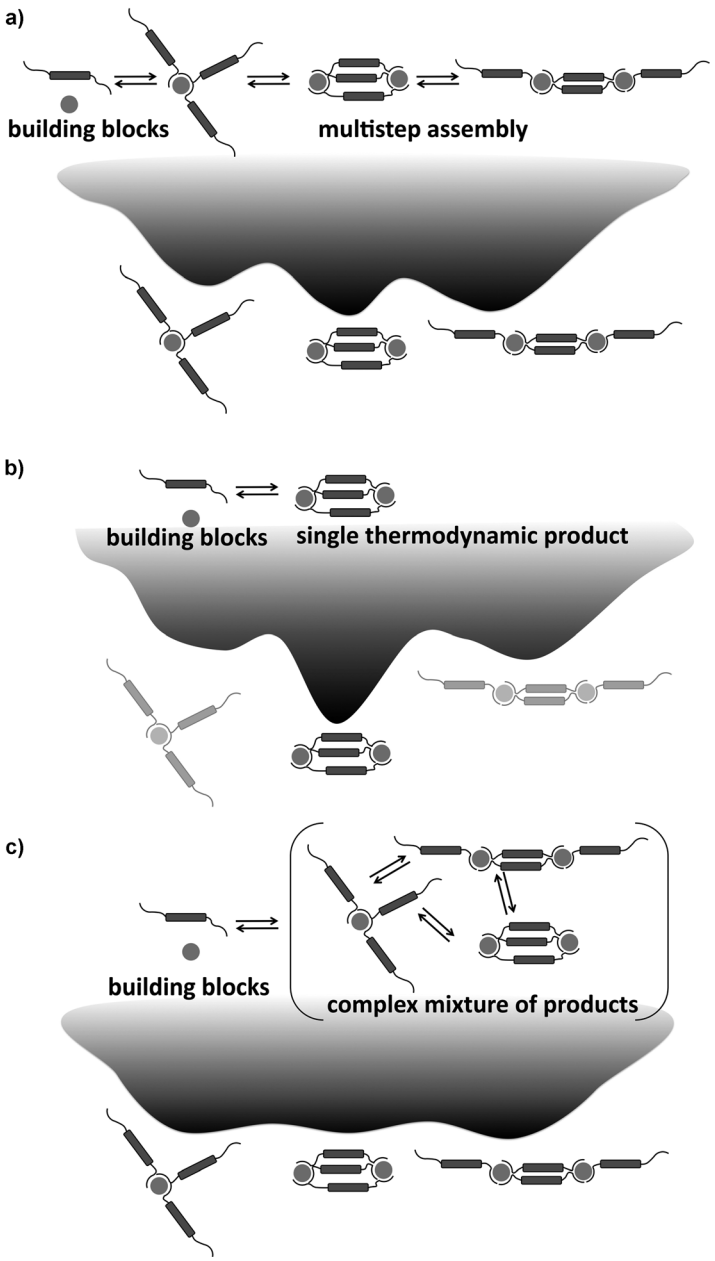

Scheme 1. Complex formation of building blocks and its free-energy landscape.

spectrum showed a subsequent change (Figure 1a, B to C).[35] Such biphasic UV/Vis spectral changes are ascribed to multistep complex formation between $\mathbf{L^1}$ and Zn^{2+}, whereby $\mathbf{L^1}$ forms two types of complex species in which structures interconvert depending on the Zn^{2+} concentration. The biphasic spectral change is also found during titration of $\mathbf{L^4}$ with Zn^{2+} (Figure 1d), thus indicating a multistep equilibrium between them.[37] However, in the titration of the monosubstituted ligand ($\mathbf{L^2}$) that contained one binding site and was capable of forming only a mononuclear Zn^{2+} complex, a successive spectral change was observed while maintaining an isosbestic point at 332 nm (Figure 1b). Similarly, $\mathbf{L^3}$ and $\mathbf{L^5}$ show one-step UV/Vis spectral changes with strict isosbestic points (Figure 1c and e, respectively). These successive spectral changes are a clear indication that these ligands ($\mathbf{L^2}$, $\mathbf{L^3}$, and $\mathbf{L^5}$) form a single complex species (thermodynamic product) with Zn^{2+}.

On the basis of the UV/Vis titration experiments (Figure 1), the binding stoichiometry of the carbazole ligands ($\mathbf{L^{1-5}}$) with Zn^{2+} was estimated. The results are shown in Figure 1f–j, in which each absorbance is plotted against the ratio of the Zn^{2+} concentration to the initial concentration of the carbazole ligands ($[Zn^{2+}]/[\mathbf{L}]_0$). In the titration of $\mathbf{L^1}$ and $\mathbf{L^4}$ with Zn^{2+} (Figure 1f and i, respectively), the titration curve reveals two breaks at around $[Zn^{2+}]/[\mathbf{L}]_0 = 0.50$ and 0.67, thus suggesting a binding stoichiometry of $[\mathbf{L}]/[Zn^{2+}] = 2:1$ and 3:2, respectively. The existence of two breaks in the titration curves is also a clear indication of two types of complex species. Conversely, in the titration curves of $\mathbf{L^3}$ and $\mathbf{L^5}$, only a single saturation point exists at $[Zn^{2+}]/[\mathbf{L}]_0 = 0.50$ (Figure 1h and j, respectively), thereby suggesting that these ligands ($\mathbf{L^3}$ and $\mathbf{L^5}$) form a single complex species with Zn^{2+} in $[\mathbf{L}]/[Zn^{2+}] = 2:1$ stoichiometry. As expected from the chemical structure of $\mathbf{L^2}$ with one imidazole unit that is capable of forming only a mononuclear species, the titration plot (Figure 1g) of $\mathbf{L^2}$ with Zn^{2+} reveals a simple 4:1 stoichiometry ($[Zn^{2+}]/[\mathbf{L}]_0 = 0.25$),

Results and Discussion

One-step versus multistep complex formation between carbazole ligands and Zn^{2+} ions

The chemical structures of all of the carbazole ligands ($\mathbf{L^{1-5}}$) used in this work are shown in Scheme 2. Initially, the complex formation of carbazole ligands with $Zn(OTf)_2$ ($OTf = OSO_2CF_3$) was investigated by UV/Vis titration (see below). Upon addition of 0–0.5 equivalents of Zn^{2+} to a solution of $\mathbf{L^1}$ ($[\mathbf{L^1}]_0 = 1.5 \times 10^{-4}$ M) in acetonitrile (MeCN), $\mathbf{L^1}$ shows UV/Vis absorption spectral changes with a clear isosbestic point observed at 375 nm (Figure 1a, A to B).[35,36] When more than 0.5 equivalents of Zn^{2+} were introduced into the solution, the absorption

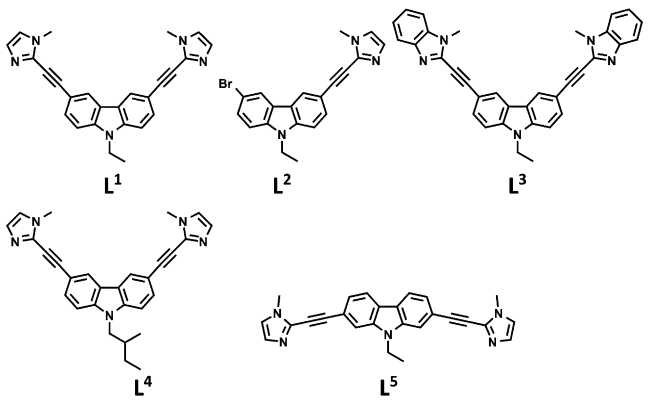

Scheme 2. Chemical structures of the carbazole ligands.

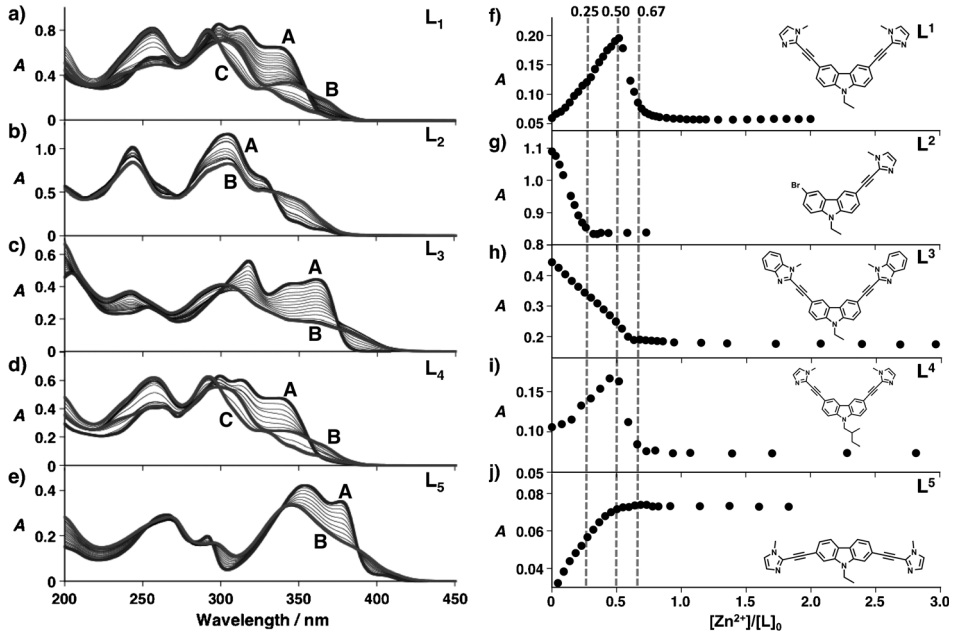

Figure 1. Observed UV/Vis absorption spectral changes upon addition of a) Zn^{2+} (A. 0 M, B. -7.8×10^{-5} M, C. -1.6×10^{-4} M) to a solution of $\mathbf{L^1}$ in MeCN (1.5×10^{-4} M); b) Zn^{2+} (A. 0 M, B. -1.7×10^{-4} M) to a solution of $\mathbf{L^2}$ in MeCN (3.1×10^{-4} M); c) Zn^{2+} (A. 0 M, B. -9.8×10^{-5} M) to a solution of $\mathbf{L^3}$ in MeCN (8.5×10^{-5} M); d) Zn^{2+} (A. 0 M, B. -6.2×10^{-5} M, C. -5.4×10^{-4} M) to a solution of $\mathbf{L^4}$ in MeCN (1.2×10^{-4} M); and e) Zn^{2+} (A. 0 M, B. -9.0×10^{-5} M) to a solution of $\mathbf{L^5}$ in MeCN (9.0×10^{-5} M) at 298 K (1 mm path length). Plots of absorbance versus $[Zn^{2+}]/[L]_0$ for the UV/Vis absorption titration of the carbazole ligands by Zn^{2+}, in which $[L]_0$ denotes the initial concentrations of $\mathbf{L^1}$–$\mathbf{L^5}$. The absorbance is monitored at f) $\lambda=365$ nm for $\mathbf{L^1}$, g) $\lambda=296$ nm for $\mathbf{L^2}$, h) $\lambda=360$ nm for $\mathbf{L^3}$, i) $\lambda=360$ nm for $\mathbf{L^4}$, and j) $\lambda=400$ nm for $\mathbf{L^5}$.

thereby suggesting the formation of a simple mononuclear complex (i.e., $(\mathbf{L^2})_4$–Zn^{2+}).[38,39]

^{1}H NMR spectroscopic characterization of complexes formed between $\mathbf{L^1}$ and Zn^{2+}

With these results in hand, the complex formation of the carbazole ligands ($\mathbf{L^{1-5}}$) with Zn^{2+} was carefully characterized by systematic NMR spectroscopic titration analysis (see below). As expected from the UV/Vis titration experiments, $\mathbf{L^1}$ also shows two-stage NMR spectral responses during the NMR spectroscopic titration (Figure 2).[35] The ^{1}H NMR spectroscopic signals of $\mathbf{L^1}$ (2.2×10^{-3} M) show broadening owing to rapid exchange between free $\mathbf{L^1}$ and that bound to Zn^{2+} in a molar ratio that ranged from $[Zn^{2+}]/[\mathbf{L^1}]_0=0.20$ to 0.45 (Figure 2). The ^{1}H NMR spectroscopic signal becomes sharp at molar ratio of around $[Zn^{2+}]/[\mathbf{L^1}]_0=0.50$, thus giving rise to a complex NMR spectrum (Figure 2).[35] The 2:1 binding stoichiometry ($[Zn^{2+}]/[\mathbf{L^1}]_0=0.50$) is consistent with that obtained from the UV/Vis titration analysis (see above, Figure 1 f). The single peak at $\delta=3.82$ ppm (Figure 2 bottom, closed square) owing to the *N*-Me protons of the imidazole rings splits into four singlet peaks at $\delta=4.07$, 3.85, 3.64, and 3.30 ppm at a molar ratio ($[Zn^{2+}]/[\mathbf{L^1}]_0$) of 0.50 (Figure 2). If $\mathbf{L^1}$ had formed a simple 2:1 complex with Zn^{2+} (i.e., $(\mathbf{L^1})_2$–Zn^{2+}), only two distinct singlet signals for the free and bound imidazole groups would have appeared. In fact, in a ^{1}H NMR spectroscopic titration of the reference compound $\mathbf{L^2}$ with one imidazole unit, $\mathbf{L^2}$ gives rise to a simple NMR spectroscopic pattern in the presence of Zn^{2+} (see Figure S2 in the Supporting Information), which is in sharp contrast to the bridging ligand $\mathbf{L^1}$. Hence, further splitting of the *N*-Me signal of $\mathbf{L^1}$ (Figure 2) indicates that two sets of $\mathbf{L^1}$ ligands are located in different chemical environments and lost their C_2 symmetry through formation of a ligand-bridged complex. In addition to this, it should be noted that the doublet peak due to the aromatic proton of the carbazole ring (C^1–H) shows a considerable upfield shift from $\delta=7.75$ to 5.73 ppm at $[Zn^{2+}]/[\mathbf{L^1}]_0=0.50$ (Figure 2). This large upfield shift clearly shows the shielding effects of the carbazole rings, a clear indication of the π-stacked carbazole units. This upfield signal disappears with increasing concentration of Zn^{2+} (Figure 2), whereby the four splitting signals due to *N*-Me protons of the imidazole groups become one peak at $\delta=2.93$ ppm (Figure 2 top, closed square). These results indicate that above the molar ratio of 0.50 ($[Zn^{2+}]/[\mathbf{L^1}]_0>0.50$), the complex with π-stacked carbazole units undergoes a structural transition to another complex that has no π-stacking carbazole ring, in which all $\mathbf{L^1}$ ligands bound to Zn^{2+} have the same chemical environments with C_2 symmetry.

To address a full characterization of these complex species, we have tried to prepare a single crystal of the complex, but the multistep equilibrium between $\mathbf{L^1}$ and Zn^{2+} makes the formation of the single crystal difficult. Finally, we obtained a small, fiberlike crystal after careful screening of suitable crystallization conditions. Single crystals were grown by the slow evaporation method at a constant temperature of 25 °C from a solution in MeCN. Unfortunately, the resolution of the X-ray crystal structure is insufficient for unambiguously deducing the position of the counteranion ($OSO_2CF_3^-$) and the solvent molecule (MeCN); however, X-ray crystallography revealed π-stacked carbazole units in the complex (not shown). In the crystal structure, $\mathbf{L^1}$ forms a three-dimensional metal–organic network architecture ($[-\mathbf{L^1}-Zn^{2+}-]_n$) with Zn^{2+},[32] in which each Zn^{2+} binds to four imidazole rings. Coordination metal–organic networks should be a result of the successive assembly process of the complex species during the crystallization (condensation) process (Scheme 3). Hence, a structure of the carbazole-bridged dinuclear complex $[(\mathbf{L^1})_4$–$(Zn^{2+})_2]$ was extracted from the crystal structure and optimized by molecular mechan-

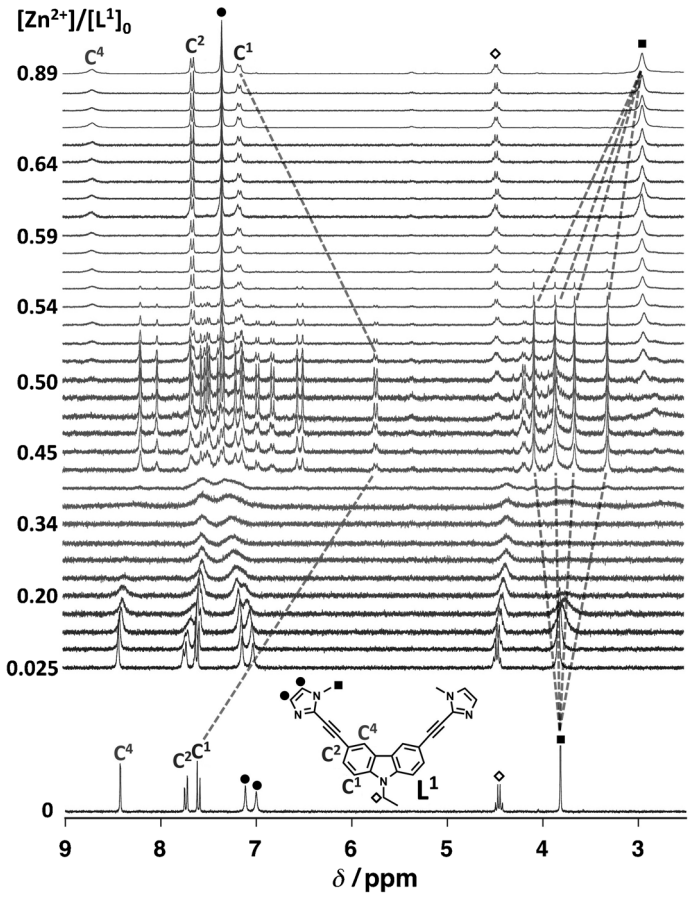

Figure 2. Stacked ^{1}H NMR spectra of $\mathbf{L^1}$ (2.2×10^{-3} M) in the presence of Zn^{2+} (0–2.0×10^{-3} M) in CD_3CN at 298 K. Numbers and symbols correspond to those in the chemical structure of $\mathbf{L^1}$.

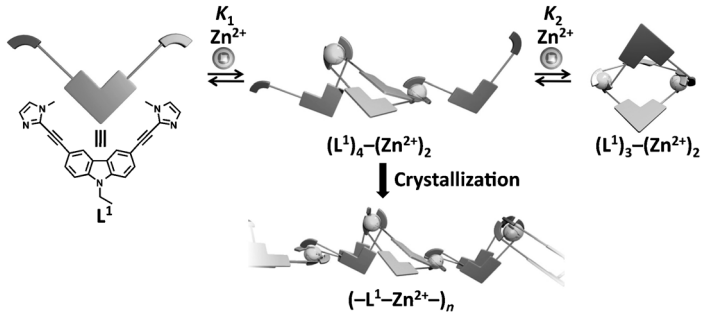

Scheme 3. Complex formation between $\mathbf{L^1}$ and Zn^{2+}.

ics (MM) (Figure 3a).[40] The model structure consists of two types of $\mathbf{L^1}$, free and π-stacked $\mathbf{L^1}$ (Figure 3a; $\mathbf{L^{1a}}$ and $\mathbf{L^{1b}}$, respectively), in which the C^1 proton of $\mathbf{L^{1a}}$ are shielded by the carbazole rings, which is consistent with the ^{1}H NMR spectroscopic assignment (see above). The partial shielding between the carbazole rings causes the loss of C_2 symmetry in the bridged $\mathbf{L^1}$ ligands ($\mathbf{L^{1a}}$). In addition, the free and bound imidazole groups in $\mathbf{L^{1b}}$ result in the loss of C_2 symmetry of $\mathbf{L^{1b}}$ (Figure 3a). As a consequence, the imidazole group is differentiated into four parts, each with different chemical environments (Figure 3a, A–D), thereby providing a quantitatively consistent explanation of the ^{1}H NMR spectroscopic data (Figure 2).

These systematic investigations have allowed us to postulate a multistep equilibrium between $\mathbf{L^1}$ and Zn^{2+} (Scheme 3). According to Scheme 3, $\mathbf{L^1}$ forms the 4:2 complex $[(\mathbf{L^1})_4$–$(Zn^{2+})_2]$ with π-stacked carbazole units at the molar ratio of $[Zn^{2+}]/[\mathbf{L^1}]_0 = 0.50$ (first step in Scheme 3), which changes to a 3:2 complex $[(\mathbf{L^1})_3$–$(Zn^{2+})_2]$ above $[Zn^{2+}]/[\mathbf{L^1}]_0 = 0.50$ (second step in Scheme 3). The $(\mathbf{L^1})_3$–$(Zn^{2+})_2$ complex has no π-stacking carbazole ring, in which three $\mathbf{L^1}$ ligands are bridged by two Zn^{2+} ions. Hence, reversible formation and dissociation of π stacking between the carbazole rings take place through a change in Zn^{2+} concentration. A model structure of $(\mathbf{L^1})_3$–$(Zn^{2+})_2$ was also created on the basis of the crystal structure.[41] The model structure has no π-stacked $\mathbf{L^1}$ ligand, and three equivalent $\mathbf{L^1}$ ligands bridge to two Zn^{2+} ions with C_2 symmetry (Figure 4), which is consistent with the ^{1}H NMR spectroscopic assignment (see above). The $(\mathbf{L^1})_3$–$(Zn^{2+})_2$ complex was also identified by ESI-MS, whereby the positive-ion ESI mass spectrum of a signal at *m/z* 818.1 corresponds to $\{Zn_2[\mathbf{L^1}]_3(OSO_2CF_3)_2\}^{2+}$ (see Figure S4 in the Supporting Information). The characteristic distribution of the isotopomer in its signals agrees closely with its calculated isotopic distributions. However, the $(\mathbf{L^1})_3$–$(Zn^{2+})_2$ complex changes to $(\mathbf{L^1})_4$–$(Zn^{2+})_2$ through dissociation and reassociation at equilibrium. The exchange rate is slow enough on the NMR spectroscopic timescale to allow two distinct signals for $(\mathbf{L^1})_4$–$(Zn^{2+})_2$ and $(\mathbf{L^1})_3$–$(Zn^{2+})_2$ (Figure 2). However, the chemical exchange is rapid on the nuclear Overhauser effect (NOE) timescale (see below). When irradiated on the doublet signals of the upfield-shifted carbazole proton of $(\mathbf{L^1})_4$–$(Zn^{2+})_2$ at $\delta = 5.73$ ppm (Figure 3b), unusually strong NOE signals were detected for the protons of $(\mathbf{L^1})_4$–$(Zn^{2+})_2$ at $\delta = 7.64$ and 7.52 ppm (4H) with the C^1 proton of $(\mathbf{L^1})_3$–$(Zn^{2+})_2$ at $\delta =$ 7.15 ppm (Figure 3d). These intense NOE signals can be assigned to rapid exchange between the carbazole ligands of the complex species on the NOE timescale through the ligand association and dissociation processes.[42] These exchange NOE peaks enable us to identify the doublet signals of $(\mathbf{L^1})_4$–$(Zn^{2+})_2$ at $\delta =$ 5.73, 7.14, and 7.52 ppm (4H) as the C^1 proton in the carbazole units.[43] The complex ^{1}H NMR spectrum of $(\mathbf{L^1})_4$–$(Zn^{2+})_2$ was successfully identified by means of the above-mentioned procedures combined with ^{1}H correlation spectroscopy (COSY) and 2D rotating-frame nuclear Overhauser effect spectroscopy (ROESY) NMR spectroscopy (see details in the Experimental Section and Figure S5 and S6 in the Supporting Information), whereby each signal of $\mathbf{L^1}$ (C^1–H, C^2–H, C^4–H, and two imidazole protons) is differentiated into four peaks (Figure 3b).[44]

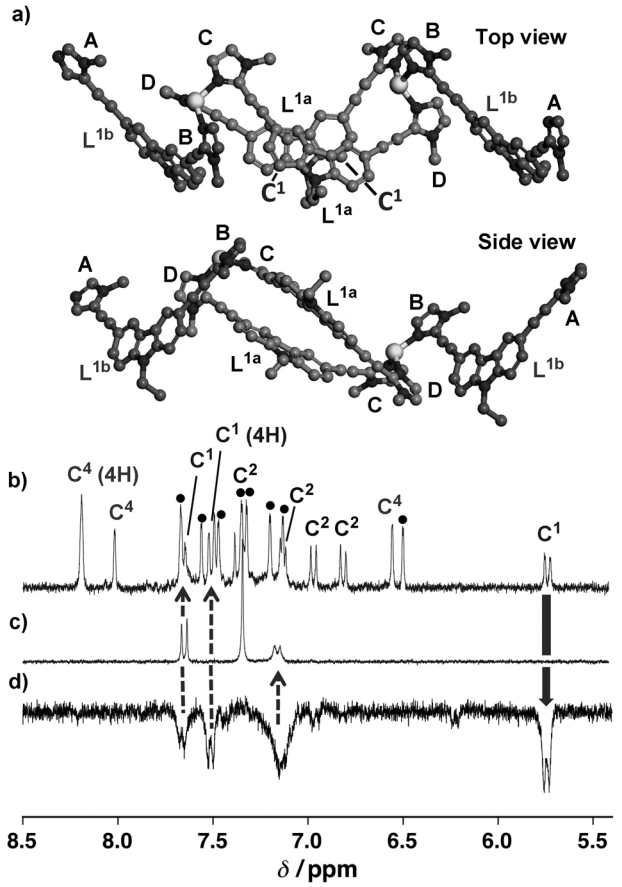

Figure 3. a) The structures of $(L^1)_4$–$(Zn^{2+})_2$ modeled by molecular mechanics (MM). A–D distinguishes imidazole moieties in different chemical environments. ^{1}H NMR spectra of b) $(L^1)_4$–$(Zn^{2+})_2$ and c) $(L^1)_3$–$(Zn^{2+})_2$ in CD_3CN at 298 K. d) NOE spectrum of a solution of L^1 in CD_3CN (4.9×10^{-2} M) in the presence of Zn^{2+} (3.0×10^{-2} M) at irradiation of the carbazole C^1 proton at $\delta = 5.73$ ppm. Numbers and symbols correspond to those in the chemical structure of L^1 and the structure of $(L^1)_4$–$(Zn^{2+})_2$.

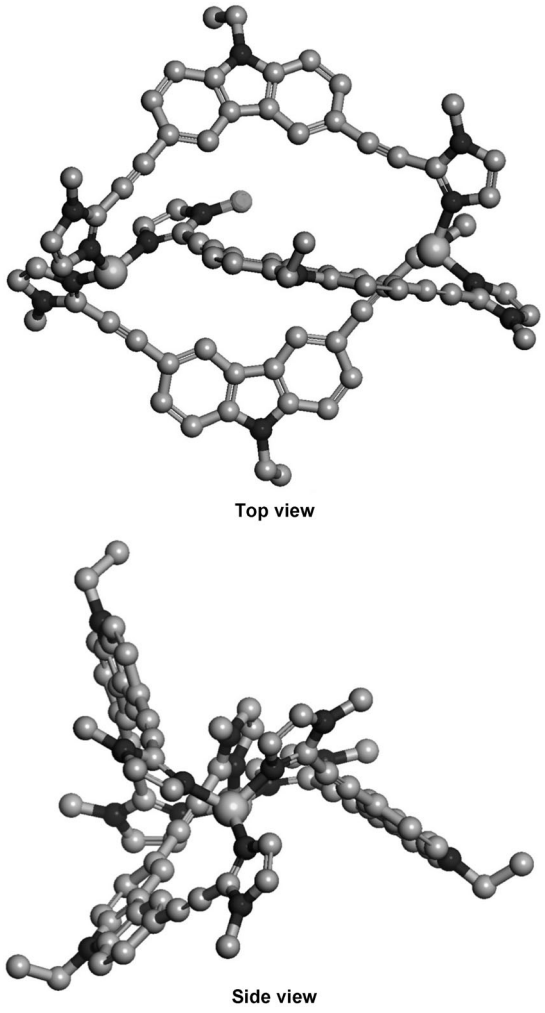

Figure 4. The structures of $(L^1)_3$–$(Zn^{2+})_2$ modeled by molecular mechanics (MM).

Thermodynamic parameters between $(L^1)_4$–$(Zn^{2+})_2$ and $(L^1)_3$–$(Zn^{2+})_2$

Evaluation of thermodynamic parameters between $(L^1)_4$–$(Zn^{2+})_2$ and $(L^1)_3$–$(Zn^{2+})_2$ should yield important insights into the multistep equilibrium between L^1 and Zn^{2+} (Scheme 3). Hence, thermodynamic parameters were extracted from NMR spectra of a solution in CD_3CN that contained constant concentrations of L^1 (2.1×10^{-3} M) and Zn^{2+} (1.8×10^{-3} M) as a function of temperature (see below). Under these conditions with the molar ratio above 0.67 ($[Zn^{2+}]/[L^1]_0 = 0.86$), almost all L^1 ligands form $(L^1)_3$–$(Zn^{2+})_2$ at 295 K, at which there is no $(L^1)_4$–$(Zn^{2+})_2$ peak in the NMR spectrum (Figure 5, bottom). However, with decreasing temperature the $(L^1)_4$–$(Zn^{2+})_2$ peak appears and its intensity increases gradually (Figure 5 from bottom to top), thereby suggesting that $(L^1)_4$–$(Zn^{2+})_2$ is enthalpically favored over $(L^1)_3$–$(Zn^{2+})_2$. The concentrations of $(L^1)_4$–$(Zn^{2+})_2$ and $(L^1)_3$–$(Zn^{2+})_2$ at each temperature were determined by the integration ratio of

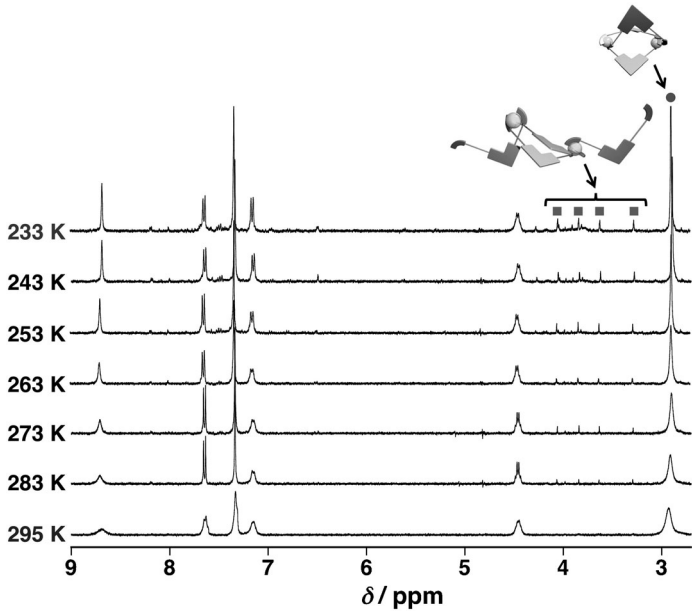

Figure 5. ^{1}H NMR spectra of L^1 (2.1×10^{-3} M) in the presence of Zn^{2+} (1.8×10^{-3} M) in CD_3CN at 233–295 K.

N-Me protons of $(\mathbf{L^1})_4$–$(Zn^{2+})_2$ and $(\mathbf{L^1})_3$–$(Zn^{2+})_2$ (Figure 5, closed circles and squares, respectively), then the equilibrium constant (K_2) was calculated from the concentrations of $(\mathbf{L^1})_4$–$(Zn^{2+})_2$, $(\mathbf{L^1})_3$–$(Zn^{2+})_2$ and free Zn^{2+} for each temperature (see Table S7 in the Supporting Information). Enthalpy (ΔH) and entropy (ΔS) for the conversion of $(\mathbf{L^1})_4$–$(Zn^{2+})_2$ into $(\mathbf{L^1})_3$–$(Zn^{2+})_2$ were obtained on the basis of temperature dependences of the K_2 value as $\Delta H = (12.7 \pm 1.9)$ kcal mol^{-1} and $\Delta S = (82.3 \pm 7.5)$ cal mol^{-1} K^{-1} (see Figure S8 in the Supporting Information). The large ΔH with positive ΔS should be a result of π stacking between the carbazole rings, thereby inducing a higher order of organization of $(\mathbf{L^1})_4$–$(Zn^{2+})_2$. In addition to this, the affinity of the free (unbound) ligand for the solvent also contributes to the large enthalpy change (see below). Apparently the conversion of $(\mathbf{L^1})_4$–$(Zn^{2+})_2$ into $(\mathbf{L^1})_3$–$(Zn^{2+})_2$ is an entropy-driven process, in which the structural transition breaks the π stacking between the carbazole rings. The free-energy change (ΔG_2) for the conversion $(\mathbf{L^1})_4$–$(Zn^{2+})_2$ to $(\mathbf{L^1})_3$–$(Zn^{2+})_2$ becomes negative (a spontaneous process) at 298 K ($\Delta G_2 = -11.6$ kcal mol^{-1}) accompanied by a contribution of positive entropy ($T\Delta S = (24.5 \pm 2.2)$ kcal mol^{-1}).

In light of these results, we can elucidate a multistep equilibrium based on a process with four states as shown in Scheme 4 (**A**–**D**).[12c,d] The equilibrium constants K_1, K_2, and K_3 are defined in Equations (1), (2), and (3), respectively.

$$4\,\mathbf{L} + 2\,Zn^{2+} \overset{\Delta G_1,\ K_1}{\rightleftharpoons} (\mathbf{L})_4\text{–}(Zn^{2+})_2 \quad (1)$$

$$3(\mathbf{L})_4\text{–}(Zn^{2+})_2 + 2\,Zn^{2+} \overset{\Delta G_2,\ K_2}{\rightleftharpoons} 4(\mathbf{L})_3\text{–}(Zn^{2+})_2 \quad (2)$$

$$(\mathbf{L})_4\text{–}(Zn^{2+})_2 \overset{\Delta G_3,\ K_3}{\rightleftharpoons} (\mathbf{L})_3\text{–}(Zn^{2+})_2 + \mathbf{L} \quad (3)$$

The ratio of complex formation (α) of $(\mathbf{L^1})_4$–$(Zn^{2+})_2$ from free $\mathbf{L^1}$ and Zn^{2+} can be expressed by Equation (4) (see Figure S9 in the Supporting Information).

$$4K_1 = \alpha[\mathbf{L}]_0^{-3}(1-\alpha)^{-4}([Zn^{2+}] - 0.5\alpha[\mathbf{L}]_0)^{-2} \quad (4)$$

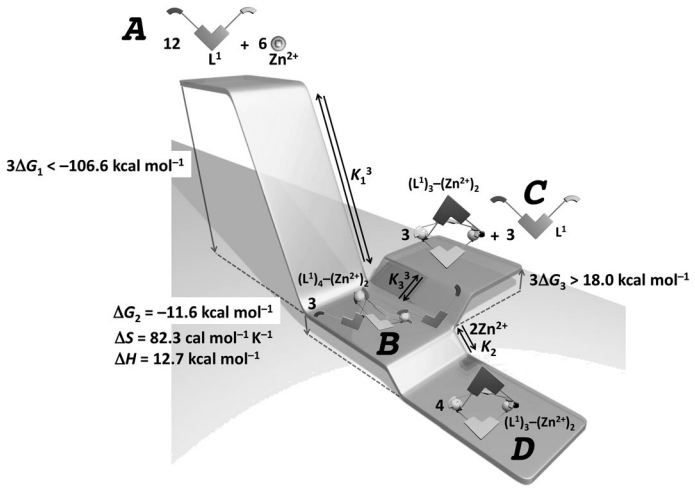

Scheme 4. Energy diagram for complex formation between $\mathbf{L^1}$ and Zn^{2+} at 298 K.

The formation constant (K_1) of $(\mathbf{L^1})_4$–$(Zn^{2+})_2$ is too large to be determined accurately, whereby formation of $(\mathbf{L^1})_4$–$(Zn^{2+})_2$ from free $\mathbf{L^1}$ and Zn^{2+} (first step in Figure 1 f) is almost stoichiometric. Such an experimental result fits the calculated curve when assuming a K_1 value larger than 1.0×10^{26} M^{-5} (see Figure S10 in the Supporting Information), which corresponds to a free-energy change $\Delta G_1 < -35.5$ kcal mol^{-1}. In contrast to the large energy difference ($3\Delta G_1 < -106.6$ kcal mol^{-1}) between **A** and **B** states, **B** and **D** lie on a practically flat potential-energy surface ($\Delta G_2 = -11.6$ kcal mol^{-1}), which corresponds to the structural transition of $(\mathbf{L^1})_4$–$(Zn^{2+})_2$ into $(\mathbf{L^1})_3$–$(Zn^{2+})_2$ with two Zn^{2+} ions. The flat potential-energy surface makes it possible to show multistep equilibrium between $\mathbf{L^1}$ and Zn^{2+}. However, conversion of state **B** to **C** (**B**→**C**) represents the structural transition of $(\mathbf{L^1})_4$–$(Zn^{2+})_2$ to $(\mathbf{L^1})_3$–$(Zn^{2+})_2$ to release free $\mathbf{L^1}$ ligands from $(\mathbf{L^1})_4$–$(Zn^{2+})_2$. The free-energy change (ΔG_3) was estimated as $\Delta G_3 > 6.0$ kcal mol^{-1} from ΔG_1 and ΔG_2 values using Equation (5) (see Figure S11 in the Supporting Information).

$$\Delta G_2 = 4\Delta G_3 + \Delta G_1 \quad (5)$$

The free-energy change for conversion of state **B** to **C**, $3\Delta G_3 > 18.0$ kcal mol^{-1}, is positive (exothermic process). Hence there is no structural transition from $(\mathbf{L^1})_4$–$(Zn^{2+})_2$ to $(\mathbf{L^1})_3$–$(Zn^{2+})_2$ at the molar ratio of $[Zn^{2+}]/[\mathbf{L^1}]_0 = 0.50$. This point is important for the carbazole ligand to be capable of forming the single thermodynamic product at each respective molar ratio ($[Zn^{2+}]/[\mathbf{L^1}]_0 = 0.50$ and 0.67). If the ΔG_3 value were negative ($\Delta G_3 < 0$), $\mathbf{L^1}$ would directly form $(\mathbf{L^1})_3$–$(Zn^{2+})_2$ in a one-step manner over the whole range of molar ratios (Scheme 5 a). Conversely, with ΔG_3 larger than $\Delta G_1/4$ ($\Delta G_3 > \Delta G_1/4$), the ΔG_2 value would be positive according to Equation (5), whereby no structural transition of $(\mathbf{L^1})_4$–$(Zn^{2+})_2$ to $(\mathbf{L^1})_3$–$(Zn^{2+})_2$ would occur (Scheme 5 b). Thus, the large formation energy (ΔG_1) of $(\mathbf{L})_4$–$(Zn^{2+})_2$ with small positive ΔG_3 ($0 < \Delta G_3 < \Delta G_1/4$) is an aspect of primary importance in the multistep equilibrium system (Scheme 5 c), in which simple adjustments to the concentration of their constituent subunits provide the single thermodynamic product at each respective molar ratio.

^{1}H NMR spectroscopic observation for complex formation of $\mathbf{L^3}$ and $\mathbf{L^4}$ with Zn^{2+}

According to Scheme 5, the thermodynamic stability of the free ligand in state **C** should be a crucial determinant of multistep or one-step equilibrium systems. Hence, the imidazole groups of $\mathbf{L^1}$ were replaced with benzoimidazole groups ($\mathbf{L^3}$) with lower affinity (solubility) for the polar solvent (MeCN). This modification should result in a larger positive ΔG_3, since the benzoimidazole groups reduce the thermodynamic stability of the unbound ligand in state **C** (Scheme 5 b). As expected from the UV/Vis titration of $\mathbf{L^3}$ with Zn^{2+} (Figures 1 c and 1 h), $\mathbf{L^3}$ shows only a one-step NMR spectroscopic spectral change as

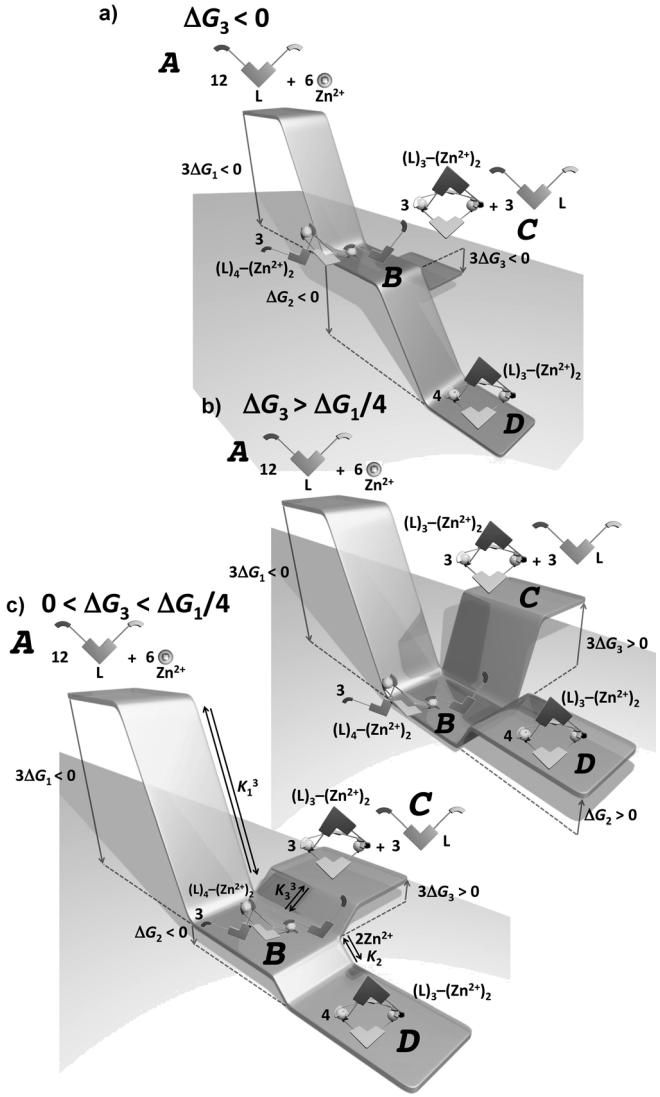

Scheme 5. Energy diagram for complex formation between the carbazole ligand (**L**) and Zn^{2+} for a) $\Delta G_3 < 0$, b) $\Delta G_3 > \Delta G_1/4$, and c) $0 < \Delta G_3 < \Delta G_1/4$.

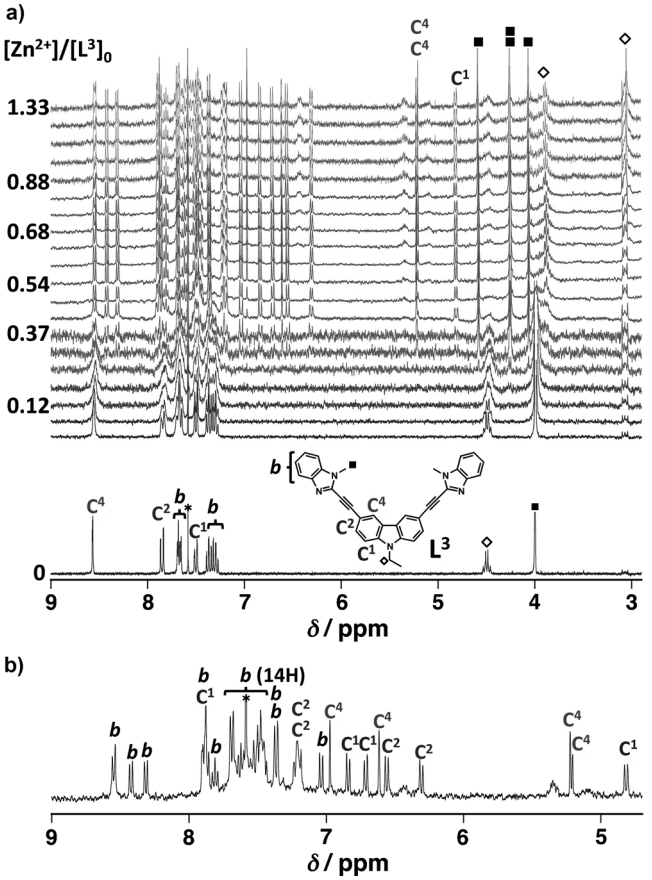

Figure 6. a) Stacked ^{1}H NMR spectra of $\mathbf{L^3}$ ($[\mathbf{L^3}]_0 = 1.0\times10^{-3}$ M) in the presence of Zn^{2+} (0–1.3×10^{-3} M) in CD_3CN at 298 K. b) ^{1}H NMR spectrum of $\mathbf{L^3}$ (1.0×10^{-3} M) in the presence of Zn^{2+} (7.2×10^{-4} M) in CD_3CN at 298 K. Numbers, characters, and symbols correspond to those in the chemical structure of $\mathbf{L^3}$.

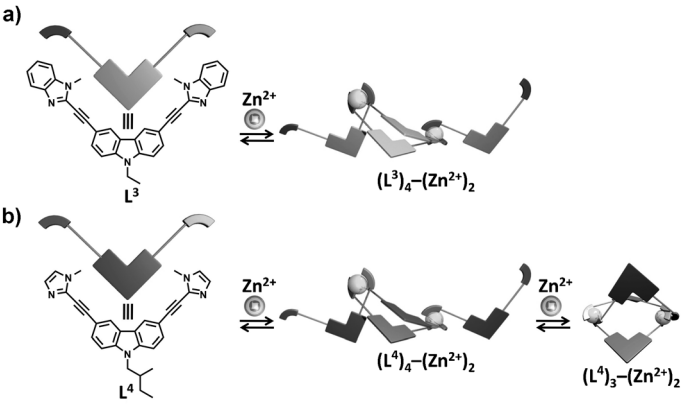

Scheme 6. Complex formation of Zn^{2+} with a) $\mathbf{L^3}$ and b) $\mathbf{L^4}$.

a function of Zn^{2+} concentration (Figure 6a), which is assignable to one-step complex formation between $\mathbf{L^3}$ and Zn^{2+} (Scheme 6a). In this case, too, the ^{1}H NMR spectroscopic signals of $\mathbf{L^3}$ show exchange broadening that arises from rapid exchange between free $\mathbf{L^3}$ and the bound ligand below a molar ratio of 0.50 $[Zn^{2+}]/[\mathbf{L^3}]_0 < 0.50$ (Figure 6a). A series of sharp NMR spectroscopic peaks are then observed at $[Zn^{2+}]/[\mathbf{L^3}]_0 = 0.50$, when almost all $\mathbf{L^3}$ ligands convert to $(\mathbf{L^3})_4$–$(Zn^{2+})_2$ (Figure 6a). In this case, no further significant spectral change is observed above the molar ratio of 0.50 $[Zn^{2+}]/[\mathbf{L^3}]_0 > 0.50$, thereby suggesting that no structural transition of $(\mathbf{L^3})_4$–$(Zn^{2+})_2$ into other complex species occurs, even at the higher molar ratio. These observations are consistent with the assumption that complex formation between $\mathbf{L^3}$ and Zn^{2+} can be categorized into Scheme 5b.

The ^{1}H NMR spectrum of $(\mathbf{L^3})_4$–$(Zn^{2+})_2$ was identified by practically the same procedures as employed in ^{1}H NMR spectroscopic characterization of $(\mathbf{L^1})_4$–$(Zn^{2+})_2$ (see Figure S12 in the Supporting Information). The result is shown in Figure 6b, in which each signal of $\mathbf{L^1}$ (C^1–H, C^2–H, C^4–H, and benzoimidazole protons) is differentiated into four peaks. Additionally, aromatic protons of the carbazole ring (C^1 and C^4) show considerable upfield shifts to $\delta = 4.82$, 5.21, and 5.23 ppm (Figure 6b), thus suggesting π stacking between the carbazole rings. Such an

NMR spectroscopic pattern is quite similar to that of $(\mathbf{L^1})_4$–$(Zn^{2+})_2$, which suggests that $\mathbf{L^1}$ forms the 4:2 complex $[(\mathbf{L^3})_4$–$(Zn^{2+})_2]$ with Zn^{2+} as a single thermodynamic product.

In the next step, the alkyl chain at the carbazole nitrogen of $\mathbf{L^1}$ was modified to replace the ethyl group ($\mathbf{L^4}$). In this case, $\mathbf{L^4}$ exhibits the biphasic NMR spectral changes that accompany complex formation with Zn^{2+} (Figure 7a), thus suggesting a multistep equilibrium between $\mathbf{L^4}$ and Zn^{2+} (Scheme 6b). The biphasic NMR spectral response is consistent with the UV/Vis titration of $\mathbf{L^4}$ with Zn^{2+} (Figures 1d and 1i). Similarly to $\mathbf{L^1}$ and $\mathbf{L^3}$ with Zn^{2+} (Figures 2 and 6a, respectively), $\mathbf{L^4}$ gives a complex NMR spectrum at the molar ratio of $[Zn^{2+}]/[\mathbf{L^4}]_0 = 0.50$ (Figure 7a), thereby suggesting the formation of $(\mathbf{L^4})_4$–$(Zn^{2+})_2$. The ^{1}H NMR spectrum of $(\mathbf{L^4})_4$–$(Zn^{2+})_2$ was also identified by virtually the same procedures as employed in ^{1}H NMR spectroscopic identification of $(\mathbf{L^1})_4$–$(Zn^{2+})_2$ and $(\mathbf{L^3})_4$–$(Zn^{2+})_2$ (see Figures S13 and S14 in the Supporting Information). The NMR spectroscopic data shows a common feature of the 4:2 complexes; each signal of $\mathbf{L^4}$ (C^1–H, C^2–H, C^4–H, and benzoimidazole protons) is differentiated into four peaks with significantly upfield-shifted carbazole proton (C^1–H), as shown in Figure 7b. The ^{1}H NMR spectroscopic signals of $(\mathbf{L^4})_4$–$(Zn^{2+})_2$ decrease above the molar ratio of $[Zn^{2+}]/[\mathbf{L^4}]_0 > 0.50$ with a concomitant appearance of new signals that arise from the formation of $(\mathbf{L^4})_3$–$(Zn^{2+})_2$, in which no clear upfield-shifted aromatic proton is detected (Figure 7a). Thus, complex formation between $\mathbf{L^4}$ and Zn^{2+} can be categorized into Scheme 5c, in which modification of the alkyl chain at the carbazole nitrogen seems to have no significant influence on the ΔG_3 value.

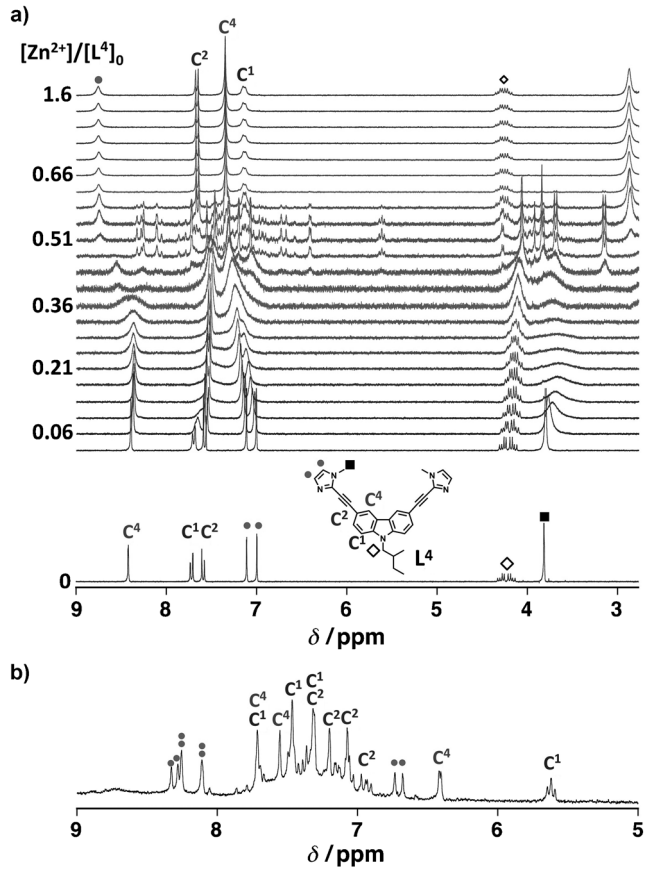

Figure 7. a) Stacked ^{1}H NMR spectra of $\mathbf{L^4}$ ($[\mathbf{L^4}]_0 = 6.0\times10^{-3}$ M) in the presence of Zn^{2+} (0–9.6×10^{-3} M) in CD_3CN at 298 K. b) ^{1}H NMR spectrum of $\mathbf{L^4}$ (8.0×10^{-3} M) in the presence of Zn^{2+} (4.3×10^{-3} M) in CD_3CN at 298 K. Numbers, characters, and symbols correspond to those in the chemical structure of $\mathbf{L^4}$.

^{1}H NMR spectroscopic observation for complex formation of $\mathbf{L^5}$ with Zn^{2+}

Finally, we investigated complex formation between $\mathbf{L^5}$ (regioisomer of $\mathbf{L^1}$) and Zn^{2+} by using ^{1}H NMR spectroscopy (Figure 8). Since the $\mathbf{L^5}$ ligand has two imidazole moieties at the 2,7-positions (in an almost linear arrangement), $\mathbf{L^5}$ should

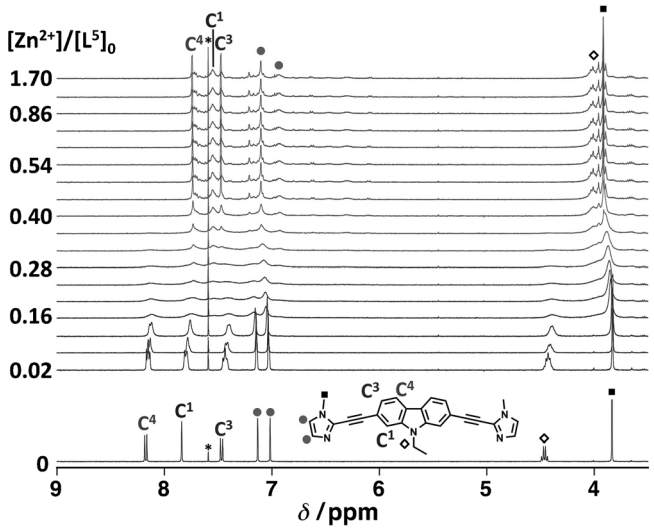

Figure 8. Stacked ^{1}H NMR spectra of $\mathbf{L^5}$ (5.0×10^{-3} M) in the presence of Zn^{2+} (0–8.5×10^{-3} M) in CD_3CN at 298 K. Numbers, characters, and symbols correspond to those in the chemical structure of $\mathbf{L^5}$.

act as a less polar ligand and have lower thermodynamic stability in the polar solvent (MeCN). ^{1}H NMR spectroscopic peaks of $\mathbf{L^5}$ gradually shift with increasing concentration of Zn^{2+}, then reaching saturation at the molar ratio of $[Zn^{2+}]/[\mathbf{L^5}]_0 = 0.50$ (Figure 8). The derived binding stoichiometry (two $\mathbf{L^5}$ ligands bound per Zn^{2+}) agrees with that obtained with the UV/Vis titration (see above, Figure 1i). In contrast to the ^{1}H NMR spectroscopic structures of the other 4:2 complexes (Figures 2b, 6b, and 7b), the complex between $\mathbf{L^5}$ and Zn^{2+} gives rise to a deceptively simple NMR spectroscopic pattern (Figure 8). In such a case, there are two possible ways to explain the simple NMR spectroscopic pattern: 1) All $\mathbf{L^5}$ ligands are located in the same chemical environments and maintain C_2 symmetry in the complex, or 2) the complex undergoes rapid dissociation and regeneration on the NMR spectroscopic timescale. For verification of this point, the complex stoichiometry of $\mathbf{L^5}$ with Zn^{2+} was also analyzed by ESI-MS, a convenient method of probing the stoichiometry and distribution of metal complexes in solutions. Intense mass signals were detected at *m/z* 817.7 $\{Zn_2[\mathbf{L^5}]_3(OSO_2CF_3)_2\}^{2+}$, 1019.3 $\{Zn_2[\mathbf{L^5}]_4(OSO_2CF_3)_2\}^{2+}$,

1200.2 $\{Zn_4[\mathbf{L^5}]_3(OSO_2CF_3)_4\}^{2+}$, 1422.4 $\{Zn[\mathbf{L^5}]_3(OSO_2CF_3)\}^{+}$, and 1784.3 for $\{Zn_2[\mathbf{L^5}]_3(OSO_2CF_3)_3\}^{+}$ (Figure 9). The mass signal at *m/z* 1019.3 corresponds to the 4:2 complex $[(\mathbf{L^5})_4{-}(Zn^{2+})_2]$, and the characteristic distribution of isotopomers in the signal

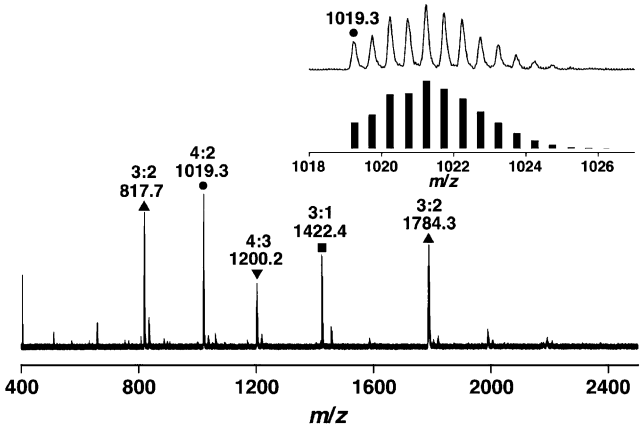

Figure 9. Positive-ion ESI-MS of a solution of $\mathbf{L^5}$ (2.6×10^{-4} M) in MeCN in the presence of Zn^{2+} (1.3×10^{-4} M). Inset: Isotopically resolved signals at *m/z* 1019.3 and the calculated isotopic distributions for $\{[Zn_2(\mathbf{L^5})_4](OSO_2CF_3)_2\}^{2+}$. Assignment: *m/z* 817.7 for $\{Zn_2[\mathbf{L^5}]_3(OSO_2CF_3)_2\}^{2+}$, 1019.3 for $\{Zn_2[\mathbf{L^5}]_4(OSO_2CF_3)_2\}^{2+}$, 1200.2 for $\{Zn_4[\mathbf{L^5}]_3(OSO_2CF_3)_4\}^{2+}$, 1422.4 for $\{Zn[\mathbf{L^5}]_3(OSO_2CF_3)\}^{+}$, and 1784.3 for $\{Zn_2[\mathbf{L^5}]_3(OSO_2CF_3)_3\}^{+}$.

agrees closely with their calculated isotopic distribution (Figure 9, inset). The other intense mass signals correspond to 3:2, 4:3, and 3:1 complexes ($(\mathbf{L^5})_3{-}(Zn^{2+})_2$, $(\mathbf{L^5})_4{-}(Zn^{2+})_3$, and $(\mathbf{L^5})_3{-}Zn^{2+}$, respectively) (see Figure S15 in the Supporting Information). Judging from the titration analysis (Figures 1i and Figure 8) in comparison with the ESI-MS spectroscopy (Figure 9), $\mathbf{L^5}$ seems to form $(\mathbf{L^5})_4{-}(Zn^{2+})_2$ as a major component with other minor complex species ($(\mathbf{L^5})_3{-}(Zn^{2+})_2$, $(\mathbf{L^5})_4{-}(Zn^{2+})_3$, and $(\mathbf{L^5})_3{-}Zn^{2+}$), in which ligand dissociation and reassociation are rapid on the NMR spectroscopic timescale (pattern 2).

Thus, complex formation between $\mathbf{L^5}$ and Zn^{2+} can be categorized under Scheme 5b, in which the substitution position of metal binding sites (2,7- or 3,6-position) is sensitive to the ΔG_3 value.

Conclusion

In this work, we have successfully demonstrated the selection criteria that determine whether molecular assembly occurs through a one-step or stepwise manner in carbazole-bridged dinuclear Zn^{2+} complex formation. The building blocks of the carbazole ligand ($\mathbf{L^1}$) with two imidazole groups at the 3,6-positions forms two types of ligand-bridged complexes, $(\mathbf{L^1})_4{-}(Zn^{2+})_2$ and $(\mathbf{L^1})_3{-}(Zn^{2+})_2$, at molar ratios ($[Zn^{2+}]/[\mathbf{L^1}]_0$) of 0.50 and 0.67, respectively. On the one hand, formation of $(\mathbf{L^1})_4{-}(Zn^{2+})_2$ provides the opportunity for π stacking between the carbazole ligands; but on the other hand, structural transition into $(\mathbf{L^1})_3{-}(Zn^{2+})_2$ results in dissociation of the π stacking. Multistep equilibrium is also observed for $\mathbf{L^4}$, which contains a 2-methylbutyl group at the carbazole nitrogen. Such multistep assembling processes are considered a primitive case of metal-assisted π-association and -dissociation processes by means of simple adjustments in the concentration of their building units. Conversely, when the imidazole groups of $\mathbf{L^1}$ are replaced with benzoimidazole groups ($\mathbf{L^3}$) with lower affinity for the polar solvent, $\mathbf{L^3}$ forms the 4:2 complex $[(\mathbf{L^3})_4{-}(Zn^{2+})_2]$ in a one-step manner, in which there is no structural transition to other complex species at the higher molar ratio. In addition, when two imidazole groups are introduced into the carbazole ring at the 2,7-positions ($\mathbf{L^5}$) to reduce the thermodynamic stability in the polar solvent, $\mathbf{L^5}$ also gives the 4:2 complex $[(\mathbf{L^5})_4{-}(Zn^{2+})_2]$ and shows no structural transition to other complex species. Thus, the simple modification of $\mathbf{L^1}$ changes the multistep to a one-step mechanism. This fact indicates that the thermodynamic stability of free building blocks is a key determinant in whether molecular assembly occurs in a one-step or multistep mechanism. Additionally, moderate thermodynamic stability of building blocks should be important for achieving a single thermodynamic product at each respective ratio of their constituent units in the multistep mechanism. This insight will open up new opportunities for creating novel supramolecular systems and their applied materials with high complexity under thermodynamic control.

Experimental Section

General

Chemicals were purchased from Wako Pure Chemical Industries Ltd. and used as received without further purification. Acetonitrile (MeCN) used as a solvent was obtained from Nacalai Tesque. Detailed synthetic procedures and characterization of $\mathbf{L^{1-5}}$ are given in the Supporting Information.

Spectral measurements

Complex formation between $\mathbf{L^{1-5}}$ and Zn^{2+} was examined from the UV/Vis spectral change of $\mathbf{L^{1-5}}$ in the presence of various concentrations of Zn^{2+} by using a Jasco V-660 spectrophotometer. The complex formation was also examined from the ^{1}H NMR spectral change of $\mathbf{L^{1-5}}$ in the presence of various concentrations of Zn^{2+} using a JEOL AL-300N FT NMR system (300 MHz). ^{1}H NMR spectroscopic assignment of the 4:2 complexes is given in the Supporting Information. The complexes formed between $\mathbf{L^5}$ and Zn^{2+} were detected by ESI-MS. Mass spectra (ESI-MS and FAB-MS) were measured using mass spectrometers (JEOL JMS-700 MStation).

Acknowledgements

This work was partly supported by a Grant-in-Aid for Young Scientists (A), Scientific Research (C) (no. 21750147), Scientific Research on Innovative Areas: "Science of Super-molecular Structures and Creation of Chemical Elements", and Scientific Research (A) (no. 21107520) from the Ministry of Education, Culture, Sports, Science and Technology, Japan.

Keywords: carbazoles · ligand effects · supramolecular chemistry · thermodynamics · zinc

[1] P. Ball, *The Self-Made Tapestry: Pattern Formation in Nature*, Oxford University Press, Oxford, **1999**.
[2] D. Philip, J. F. Stoddart, *Angew. Chem. Int. Ed. Engl.* **1996**, *35*, 1155.
[3] C. R. South, C. Burd, M. Weck, *Acc. Chem. Res.* **2007**, *40*, 63.
[4] J.-M. Lehn, A. V. Eliseev, *Science* **2001**, *291*, 2331.
[5] a) S. J. Rowan, S. J. Cantrill, G. R. L. Cousins, J. K. M. Sanders, J. F. Stoddart, *Angew. Chem.* **2002**, *114*, 938; *Angew. Chem. Int. Ed.* **2002**, *41*, 898; b) F. Cougnon, J. Sanders, *Acc. Chem. Res.* **2012**, *45*, 2211.
[6] a) S. Otto, R. L. E. Furlan, J. K. M. Sanders, *Science* **2002**, *297*, 590; b) P. T. Corbett, J. Leclaire, L. Vial, K. R. West, J.-L. Wietor, J. K. M. Sanders, S. Otto, *Chem. Rev.* **2006**, *106*, 3652; c) R. A. R. Hunta, S. Otto, *Chem. Commun.* **2011**, *47*, 847; d) S. Otto, *Acc. Chem. Res.* **2012**, *45*, 2200.
[7] A. V. Davis, R. M. Yeh, K. N. Raymond, *Proc. Natl. Acad. Sci. USA* **2002**, *99*, 4793.
[8] a) R. S. K. Kishore, V. Kalsani, M. Schmittel, *Chem. Commun.* **2006**, 3690; b) K. Mahata, M. Schmittel, *J. Am. Chem. Soc.* **2009**, *131*, 16544.
[9] a) S. Hiraoka, T. Yi, M. Shiro, M. Shionoya, *J. Am. Chem. Soc.* **2002**, *124*, 14510; b) K. Harano, S. Hiraoka, M. Shionoya, *J. Am. Chem. Soc.* **2007**, *129*, 5300.
[10] T. Haino, T. Fujii, A. Watanabe, U. Takayanagi, *Proc. Natl. Acad. Sci. USA* **2009**, *106*, 10477.
[11] Structural diversity can also be achieved by kinetic trapping of different molecular assemblies based on a single building block. See: Y. Tidhar, H. Weissman, S. G. Wolf, A. Gulino, B. Rybtchinski, *Chem. Eur. J.* **2011**, *17*, 6068.
[12] a) T. Ogawa, J. Yuasa, T. Kawai, *Angew. Chem.* **2010**, *122*, 5236; *Angew. Chem. Int. Ed.* **2010**, *49*, 5110; b) J. Yuasa, A. Mitsui, T. Kawai, *Chem. Commun.* **2011**, *47*, 5807; c) N. Inukai, T. Kawai, J. Yuasa, *Chem. Commun.* **2011**, *47*, 9128; d) N. Inukai, T. Kawai, J. Yuasa, *Chem. Eur. J.* **2013**, *19*, 5938.
[13] a) J. Yuasa, S. Fukuzumi, *J. Am. Chem. Soc.* **2006**, *128*, 15976; b) J. Yuasa, S. Fukuzumi, *J. Am. Chem. Soc.* **2008**, *130*, 566.
[14] a) P. N. W. Baxter, *Chem. Eur. J.* **2002**, *8*, 5250; b) P. N. W. Baxter, *Chem. Eur. J.* **2003**, *9*, 2531.
[15] S. Goswami, D. Sen, N. K. Das, *Org. Lett.* **2010**, *12*, 856.
[16] a) S. Akine, S. Hotate, T. Nabeshima, *J. Am. Chem. Soc.* **2011**, *133*, 13868; b) S. Akine, S. Sairenji, T. Taniguchi, T. Nabeshima, *J. Am. Chem. Soc.* **2013**, *135*, 12948.
[17] a) J. Yuasa, T. Suenobu, S. Fukuzumi, *J. Am. Chem. Soc.* **2003**, *125*, 12090; b) J. Yuasa, S. Fukuzumi, *Org. Biomol. Chem.* **2004**, *2*, 642; c) J. Yuasa, T. Suenobu, S. Fukuzumi, *J. Phys. Chem. A* **2005**, *109*, 9356.
[18] I. C. Pintre, S. Pierrefixe, A. Hamilton, V. Valderrey, C. Bo, P. Ballester, *Inorg. Chem.* **2012**, *51*, 4620.
[19] J. Etxebarria, A. Vidal-Ferran, P. Ballester, *Chem. Commun.* **2008**, 5939.
[20] V. V. Borovkov, J. M. Lintuluoto, Y. Inoue, *Org. Lett.* **2002**, *4*, 169.
[21] S. E. Boiadjiev, D. A. Lightner, *J. Am. Chem. Soc.* **2000**, *122*, 378.
[22] J.-M. Lehn, *Supramolecular Chemistry*, VCH, Weinheim, **1995**.
[23] G. M. Whitesides, B. Grzybowski, *Science* **2002**, *295*, 2418.
[24] C. Piguet, G. Bernardinelli, G. Hopfgartner, *Chem. Rev.* **1997**, *97*, 2005.
[25] M. Albrecht, *Chem. Rev.* **2001**, *101*, 3457.
[26] M. J. Hannon, L. J. Childs, *Supramol. Chem.* **2004**, *16*, 7.
[27] M. Albrecht, R. Fröhlich, *Bull. Chem. Soc. Jpn.* **2007**, *80*, 797.
[28] B. H. Northrop, Y. Zheng, K.-W. Chi, P. J. Stang, *Acc. Chem. Res.* **2009**, *42*, 1554.
[29] R. Chakrabarty, P. S. Mukherjee, P. J. Stang, *Chem. Rev.* **2011**, *111*, 6810.
[30] J. Vicente, J. Gil-Rubio, N. Barquero, V. Cámara, N. Masciocchi, *Chem. Commun.* **2010**, *46*, 1053.
[31] Carbazole derivatives have been extensively utilized as building blocks for metal–organic network architectures. See: a) J.-R. Li, H.-C. Zhou, *Angew. Chem.* **2009**, *121*, 8617; *Angew. Chem. Int. Ed.* **2009**, *48*, 8465; b) J.-R. Li, H.-C. Zhou, *Nat. Chem.* **2010**, *2*, 893; c) J.-R. Li, A. Yakovenko, W. Lu, D. Timmons, W. Zhuang, D. Yuan, H.-C. Zhou, *J. Am. Chem. Soc.* **2010**, *132*, 17599; d) W. Lu, D. Yuan, T. A. Makal, J.-R. Li, H.-C. Zhou, *Angew. Chem.* **2012**, *124*, 1612; *Angew. Chem. Int. Ed.* **2012**, *51*, 1580.
[32] H.-J. Liu, X.-T. Tao, J.-X. Yang, Y.-X. Yan, Y. Ren, H.-P. Zhao, Q. Xin, W.-T. Yu, M.-H. Jiang, *Cryst. Growth Des.* **2008**, *8*, 259.
[33] E. T. Spielberg, W. Plass, *Eur. J. Inorg. Chem.* **2011**, 826.
[34] The π-stacking interaction is one of the most common noncovalent interaction motifs. It determines the function and structure of the molecular assemblies. See: a) W. Saenger, *Principles of Nucleic Acid Structure*, Springer, New York, **1984**; b) D. B. Amabilino, J. F. Stoddart, *Chem. Rev.* **1995**, *95*, 2725; c) H. W. Roesky, M. Andruh, *Coord. Chem. Rev.* **2003**, *236*, 91.
[35] Some preliminary results on stepwise complex formation between $\mathbf{L^1}$ and Zn^{2+} have appeared. See: N. Inukai, J. Yuasa, T. Kawai, *Chem. Commun.* **2010**, *46*, 3929.
[36] The clear isosbestic point indicates that all $\mathbf{L^1}$ ligands convert the single complex, that is, $(\mathbf{L^1})_4$–$(Zn^{2+})_2$ at a molar ratio of $[Zn^{2+}]/[\mathbf{L^1}]_0 = 0.50$.
[37] Because $\mathbf{L^4}$ has a chiral alkyl group at the carbazole nitrogen, we also examined the circular dichroism (CD) spectral analysis of $\mathbf{L^4}$ with Zn^{2+}. Although $\mathbf{L^4}$ shows no detectable CD signal in the absence of Zn^{2+} (see Figure S1 in the Supporting Information), successive addition induces intense CD bands in the spectral range of the π–π^* transition of the carbazole ligand. The intense CD signal should arise from the exciton coupling of the bridging carbazole units in the dinuclear complex.
[38] The 4:1 complex formation between $\mathbf{L^2}$ and Zn^{2+} was also confirmed by ^{1}H NMR spectroscopic titration (see Figure S2 in the Supporting Information).
[39] The binding stoichiometries were also determined by Job plots for $\mathbf{L^1}$–$\mathbf{L^5}$ with Zn^{2+} (see Figure S3 in the Supporting Information). The determined stoichiometries are same as those determined by UV/Vis titration (Figure 1) and ^{1}H NMR spectroscopic titration (Figures 2, 6–8).
[40] In the preliminary study, we tentatively concluded that $\mathbf{L^1}$ forms a dimer complex with Zn^{2+}. As part of a continuing investigation, we obtained the crystal structure of the Zn^{2+} complex with $\mathbf{L^1}$ (not shown) and reevaluated the binding stoichiometry between $\mathbf{L^1}$ and Zn^{2+}. This systematic investigation has allowed us to conclude that $\mathbf{L^1}$ forms $(\mathbf{L^1})_4$–$(Zn^{2+})_2$. It should be noted that we have provided the additional supplementary materials in the preliminary study; see ref. [35].
[41] Although the species at high Zn^{2+} concentration is difficult to assign with certainty from the simple NMR spectroscopic pattern (Figure 2) and there might be other possible assignments, we tentatively assigned the complex at high Zn^{2+} concentration as $(\mathbf{L})_3$–M_2-type bridging complexes from the titration analysis and ESI-MS detection. For recent examples of $(\mathbf{L})_3$–M_2-type bridging complexes, see: a) N. Kundu, M. Maity, P. B. Chatterjee, S. J. Teat, A. Endo, M. Chaudhury, *J. Am. Chem. Soc.* **2011**, *133*, 20104; b) T. Haino, H. Shio, R. Takano, Y. Fukazawa, *Chem. Commun.* **2009**, 2481; c) B. Birkmann, A. W. Ehlers, R. Fröhlich, K. Lammertsma, F. E. Hahn, *Chem. Eur. J.* **2009**, *15*, 4301; d) E. Terazzi, L. Guénée, B. Bocquet, J.-F. Lemonnier, N. D. Favera, D. Piguet, *Chem. Eur. J.* **2009**, *15*, 12719.
[42] E. Alessio, L. Hansen, M. Iwamoto, L. Marzilli, *J. Am. Chem. Soc.* **1996**, *118*, 7593.
[43] These exchange NOE signals were further confirmed by 2D ROESY NMR spectrum (red dashed lines in Figure S5 in the Supporting Information), in which red spots in the 2D ROESY show negative chemical exchange peaks. No ROE peak was observed under these conditions ($\mathbf{L^1}$ (2.0×10^{-3} M) and Zn^{2+} (1.0×10^{-3} M)). 2D ROESY of free $\mathbf{L^1}$ (2.0×10^{-3} M) is also given Figure S5 in the Supporting Information.
[44] 2D DOSY spectra of $(\mathbf{L^1})_4$–$(Zn^{2+})_2$ and $(\mathbf{L^1})_3$–$(Zn^{2+})_2$ are given in Figures S16 and S17 of the Supporting Information. All ^{1}H signals of $(\mathbf{L^1})_4$–$(Zn^{2+})_2$ (green squares in Figure S16 in the Supporting Information) have the same diffusion coefficient ($D = 1.5\times10^{-9}$ m^2 s^{-1}, $\sigma = 0.01750$). This result supports that the complicated ^{1}H signals do not originate from the mixture of other complexes in the ratio of 2:1 (i.e., $(\mathbf{L})_2$–Zn^{2+}, $(\mathbf{L})_6$–$(Zn^{2+})_3$, $(\mathbf{L})_8$–$(Zn^{2+})_4$, and so on). As expected, the diffusion coefficient ($D = 1.3\times10^{-9}$ m^2 s^{-1}, $\sigma = 0.01756$) of $(\mathbf{L^1})_3$–$(Zn^{2+})_2$ determined from the 2D DOSY spectra is close to that of $(\mathbf{L^1})_4$–$(Zn^{2+})_2$ ($D = 1.5\times10^{-9}$ m^2 s^{-1}), thus indicating that the size of the $(\mathbf{L^1})_4$–$(Zn^{2+})_2$ is not so different from that of $(\mathbf{L^1})_3$–$(Zn^{2+})_2$.

Received: April 11, 2014
Revised: July 4, 2014
Published online on September 18, 2014